

Aspects of the momentum dependence of the equation of state and of the residual NN cross section, and their effects on nuclear stopping

Z. Basrak^{1,*}, P. Eudes^{2,†} and V. de la Mota²

¹*Ruđer Bošković Institute, Zagreb, Croatia and*

²*SUBATECH, EMN-IN2P3/CNRS-Université de Nantes, Nantes, France*

(Dated: September 10, 2018)

With the semiclassical Landau-Vlasov transport model we studied the stopping observable R_E , the energy-based isotropy ratio, for the $^{129}\text{Xe} + ^{120}\text{Sn}$ reaction at beam energies spanning $12A$ to $100A$ MeV. We investigated the impacts of the nonlocality of the nuclear mean field, of the in-medium modified nucleon-nucleon (NN) cross section and of the reaction centrality. A fixed set of model parameters yields R_E values that favorably compare with the experimental ones, but only for energies below the Fermi energy E_F . Above E_F agreement is readily possible, but by a smooth evolution with energy of the parameter that controls the in-medium modification of NN cross section. By comparing the simulation correction factor \mathcal{F} applied to the free NN cross section with the one deduced from experimental data [Phys. Rev. C **90**, 064602 (2014)], we infer that the zero-range mean field almost entirely reproduces it. Also, in accordance with what has been deduced from experimental data, around E_F a strong reduction of the free NN cross section is found. In order to test the impact of sampling central collisions by multiplicity an event generator (HIPSE) was used. We obtain that high multiplicity events are spread over a broad impact parameter range, but it turns out that this has a small effect on the observable R_E and, thus, on \mathcal{F} as well.

PACS numbers: 25.70.-z, 21.30.-x, 24.10.Lx

I. INTRODUCTION

The ratio between transverse and longitudinal components of kinematical observables is a measure of the conversion of the initial entrance channel motion into intrinsic degrees of freedom in heavy-ion collisions (HICs). Such an observable gives an insight on the rate of a system's equilibration, of the dissipation of the available energy, as well as of HIC stopping power [1, 2]. Thanks to such an observable, the FOPI Collaboration has evidenced partial nuclear transparency in HIC in the beam-energy range $E_{\text{inc}} \approx 0.1A - 1A$ GeV [3]. More recently, by examining the ratio of transverse to longitudinal energy R_E and linear momentum R_p for the most violent HICs, the INDRA Collaboration has revealed a substantial reduction of the nuclear stopping power at $E_{\text{inc}} \approx 10A - 100A$ MeV [4]. This stopping observable reaches a minimum around the Fermi energy E_F and stagnates or very weakly increases with the further increase of E_{inc} at least up to $100A$ MeV, the upper limit of the energy range available in this study. The above observation is valid for all (mass symmetric) systems studied, with system masses $A_{\text{sys}} = 72 - 394$ a.m.u. It is worth emphasizing that the fusion cross section normalized by the total reaction cross section exhibits an analogously rapid fall-off up to about E_F [5, 6], a behavior especially evident for mass-symmetric systems (cf. Fig. 6 of Ref. [6]).

In a recent publication [7] the above observable R_E was analyzed for the $Z=1$ subset of the same INDRA data. The $Z=1$ R_E displays a slightly stronger increase

with $E_{\text{inc}} > E_F$ for the heavier systems [7] relative to the R_E values obtained in the previous study [4] which included light charged particles and fragments, but also was somewhat more stringent on the selection of the most central events. The authors of Ref. [7] report a minimum of R_E around E_F , which is particularly enhanced when R_E is normalized to the Fermi-gas-model prediction of the incoming R_E value at a given E_{inc} . [8]

In Ref. [7] it was assumed that protons are predominantly dynamically emitted during the early reaction phase, in accordance with Refs. [9, 10]. Such a hypothesis offers a possibility of extracting information on the in-medium correction for the free nucleon-nucleon (NN) cross section $\sigma_{\text{NN}}^{\text{free}}$. Following such an argument, starting from the experimental R_E values in Ref. [7], with some basic assumptions about the effects owing to the Pauli-exclusion principle, the nucleon mean free path was extracted and an effective value of the in-medium NN cross section σ_{NN}^m was deduced. In the process, a correction factor \mathcal{F} was obtained by which $\sigma_{\text{NN}}^{\text{free}}$ has to be multiplied at each E_{inc} to get a proper σ_{NN}^m value. The authors found that (i) a *significant reduction* of $\sigma_{\text{NN}}^{\text{free}}$ is present in HICs below $100A$ MeV and (ii) this change of $\sigma_{\text{NN}}^{\text{free}}$ is strongly dependent upon E_{inc} . At the lowest energies the measured R_E is compatible with the full stopping value ($R_E \approx 1$) and the effective σ_{NN}^m amounts to about $0.4 \sigma_{\text{NN}}^{\text{free}}$. One should keep in mind that the authors claimed a large uncertainty on the factor \mathcal{F} below $E_{\text{inc}} \sim 30A$ MeV, a subject for which they have announced a devoted publication [7]. At incident energies around E_F where R_E attains its minimum, σ_{NN}^m is reduced to less than one fifth the free $\sigma_{\text{NN}}^{\text{free}}$ value ($\mathcal{F} = 0.17$) and then the effective σ_{NN}^m steadily and regularly increases up to half of the free value ($\mathcal{F} \approx 0.5$) at

* basrak@irb.hr

† eudes@subatech.in2p3.fr

$E_{\text{inc}} = 100A$ MeV [7] (see also Fig. 3 in the present work).

The stopping observables R_E and/or R_p have also been investigated in isospin-dependent quantum molecular dynamics (IQMD) [8, 11–14] and antisymmetrized molecular dynamics (AMD) [15] model studies of HICs. All these works were carried out before publication of Ref. [7]. Neither of simulation approaches predicts the remarkable in-medium reduction of $\sigma_{\text{NN}}^{\text{free}}$ found in Ref. [7]. In the AMD study, specific attention has been paid to performing the analysis by meticulously following the experimental procedure for data handling [15]. The simulation with in-medium σ_{NN} due to Li and Machleidt [16] (the free σ_{NN}) undershoots (overshoots) the data of [4]. An agreement with the data could only be reached at $E_{\text{inc}} \geq 80A$ MeV by doubling the theoretically established σ_{NN}^m of [16]. A systematic investigation of the impact of σ_{NN} on R_E , however, has not been performed yet. The intention of the present study is twofold:

1. by varying the nuclear equation of state (EOS) and the parametrization of σ_{NN} , to investigate how the semiclassical Landau-Vlasov (LV) transport model of HIC [17, 18] complies with the experimentally deduced dependence of the stopping observable R_E on E_{inc} and
2. by varying a simple multiplicative factor \mathcal{F} of the free NN cross section, to compare thus obtained values for \mathcal{F} with those reported in Ref. [7].

II. MODEL INGREDIENTS

Within the semiquantal extension of the Boltzmann transport theory, the highly nonlinear LV equation governs the spatio-temporal evolution of the one-body density distribution function $f(\mathbf{r}, \mathbf{p}; t)$:

$$\frac{\partial f(\mathbf{r}, \mathbf{p}; t)}{\partial t} + \{f(\mathbf{r}, \mathbf{p}; t), H\} = I_{\text{coll}}(f(\mathbf{r}, \mathbf{p}; t)), \quad (1)$$

which gives the probability of finding at the instant t a particle in the phase-space point (\mathbf{r}, \mathbf{p}) . $\{, \}$ stands for the Poisson bracket, whereas H is the one-body Hamiltonian describing the Coulomb potential and the nuclear mean field. We present the results obtained with a soft nonlocal mean field labeled D1-G1 ($K_\infty = 228$ MeV, $m^*/m = 0.67$) due to Gogny [19] and those obtained with the standard simplification of the soft zero-range Skyrme interaction due to Zamick ($K_\infty = 200$ MeV, $m^*/m = 1.0$) [20]. The D1-G1 force is reputed to reproduce fundamental properties of nuclear matter as well as those of finite nuclei [19] while the Zamick parametrization of the EOS is, owing to its simplicity, of rather widespread use in a number of microscopic approaches. Details on both the nonlocal and the local parametrizations of the used EOS may be found in Tables I and III of Ref. [21], respectively. We have demonstrated that the LV model is able to correctly describe experimental observations in the intermediate energy regime [9, 10, 18, 21, 22]. The use of only a density dependent EOS is legitimated by the finding [11, 14] that the isospin dependence of the

mean field has a weak, if any, influence on isotropy ratios. Experimental R_E 's for a number of HICs between various xenon and tin isotopes corroborate this result; cf. Table I of Ref. [4].

The function f is expanded onto a moving basis of coherent states taken as normalized Gaussians \mathcal{G}_χ (\mathcal{G}_ϕ) with frozen width χ (ϕ) in \mathbf{r} (\mathbf{p}) space:

$$f(\mathbf{r}, \mathbf{p}; t) = \frac{A}{N} \sum_i \mathcal{G}_\chi(\mathbf{r} - \mathbf{r}_i) \mathcal{G}_\phi(\mathbf{p} - \mathbf{p}_i). \quad (2)$$

A is the system mass number and N is the number of coherent states (N/A equals 60 in the present study). The widths χ and ϕ are chosen such as to best reproduce the nuclear ground state characteristics of the two colliding nuclei. The local density reads

$$\rho(\mathbf{r}) = \int d^3\mathbf{p} f(\mathbf{r}, \mathbf{p}). \quad (3)$$

Gaussians move in the self-consistent mean field and suffer hard scattering between them, controlled by the Uehling-Uhlenbeck collision integral accounting for the fermionic character of interacting particles [23]:

$$\begin{aligned} I_{\text{coll}} = & \frac{4g}{m^2} \int d^3\mathbf{p}_2 d^3\mathbf{p}_3 d^3\mathbf{p}_4 \frac{d\sigma_{\text{NN}}^m}{d\Omega} \\ & \times \delta(\mathbf{p} + \mathbf{p}_2 - \mathbf{p}_3 - \mathbf{p}_4) \delta(\epsilon + \epsilon_2 - \epsilon_3 - \epsilon_4) \\ & \times [(1 - \bar{f})(1 - \bar{f}_2)f_3f_4 - (1 - \bar{f}_3)(1 - \bar{f}_4)f_2f], \end{aligned} \quad (4)$$

which takes into account energy and momentum conservation as well as the Pauli exclusion principle. Here, m denotes the nucleonic mass, $\bar{f} = (2\pi\hbar)^3 f(\mathbf{r}, \mathbf{p}; t)/g$ is the occupation number with g the spin-isospin degeneracy [18], \mathbf{p} and \mathbf{p}_2 (\mathbf{p}_3 and \mathbf{p}_4) are initial (final) momenta of the scattering particle pair, $\epsilon = \epsilon(p)$ is the single-particle energy, while σ_{NN}^m is the *in-medium* nucleonic cross section. σ_{NN}^m is scaled so that a Gaussian-averaged mean-free path is the same as for a nucleon. The cross section dependence on isospin has been reported as crucial for the study of stopping [11]. This kind of σ_{NN} parametrization was proposed by Chen *et al.* [24], which hereafter we label $\sigma_{\text{NN}}^{\text{Chen}}$. This phenomenological $\sigma_{\text{NN}}^{\text{free}}$ is based on the empirical isospin and energy dependence of the free NN scattering and has been used in both [7] and [11]. σ_{NN} due to Li and Machleidt [16], which accounts for the in-medium effects and is also isospin dependent, is tested too.

III. RESULTS AND DISCUSSION

Our stopping observable, the energy-based isotropy ratio, is defined as the ratio between transverse E_{tran} and longitudinal E_{long} energy components of reaction ejectiles [4, 7]

$$R_E = \frac{\sum E_{\text{tran}}^i}{2 \sum E_{\text{long}}^i}, \quad (5)$$

where summation runs over particles of those reaction events that satisfy certain selection criteria. For the LV simulation results, the summation index i of Eq. (5) runs over the free Gaussians, i.e., those which are not bound in large (residue-like) fragment(s). Among the experimentally studied systems, the $^{129}\text{Xe} + ^{120}\text{Sn}$ reaction has been measured at by far the most abundant number of E_{inc} values [4, 7]. Consequently, in the present work only the simulation of this system is performed. To acquire stable R_E^{sim} values, the simulation is carried out up to 600 fm/c at the lowest $E_{\text{inc}} = 12A - 32A$ MeV and up to 240 fm/c at the highest $E_{\text{inc}} = 80A - 100A$ MeV. Beyond that time the calculation was continued until 8000 fm/c, considering only the Coulomb repulsion due to reaction residues. Special care was taken in order to perform our analysis of simulation data as close as possible to experimental conditions.

A. A density-dependent NN cross section

In the experimental analysis [7], event selection is based on the charged particle's multiplicity. The authors selected the most central events that are estimated, in cross-section units, to be equivalent to 50 to 150 mb [7]. We adopt the median value of 100 mb for our analysis. This amount corresponds to about 2% of the total reaction cross section σ_R and, in a geometrical sharp-cut approximation, to $b \leq 2.0$ fm. Consequently, in this subsection our simulation is limited to $b \leq 2.0$ fm.

Figure 1 displays R_E^{sim} obtained with the momentum-dependent D1-G1 EOS (upper panel) and with the zero-range Zamick EOS (lower panel) for several parametrizations of the in-medium corrected σ_{NN} . For comparison, the experimental R_E^{exp} 's are shown by filled circles with the corresponding errors [7]. As a reference, the R_E^{sim} results obtained with the in-medium *uncorrected* empirical free scattering $\sigma_{\text{NN}}^{\text{free}} = \sigma_{\text{NN}}^{\text{Chen}}$ [24] are displayed by the heavy dotted curves. This empirical σ_{NN} is used as an input for the in-medium modified σ_{NN}^m suggested by Cugnon *et al.* [25]. In their Brueckner G -matrix in-medium renormalization of the NN interaction, they obtained a set of parameters explicitly describing the dependence of $\sigma_{\text{NN}}^{\text{Cugnon}}$ on the local density [25]. These simulation results are displayed by the red curves and reddish zone in Fig. 1: the zone shows the range of the R_E^{sim} values limited by the impact parameters $b = 1$ fm (dashed bordering curve) and $b = 2$ fm (full bordering curve). ($b = 0$ fm has no weight and R_E^{sim} at most of energies is roughly the same for $b = 0$ and 1 fm.) The heavy curve in each zone represents the b -weighted R_E^{sim} value in the range $b = 0 - 2$ fm and corresponds to 2% of σ_R . For both EOS, the R_E^{sim} values with $\sigma_{\text{NN}}^{\text{Cugnon}}$ are very similar to those obtained with $\sigma_{\text{NN}}^{\text{Chen}}$ (dotted curves). Clearly, in the full energy range investigated here the in-medium effects of $\sigma_{\text{NN}}^{\text{Cugnon}}$ have rather weak impact on the R_E observable. Consequently, as for $\sigma_{\text{NN}}^{\text{Chen}}$, the compatibility of R_E^{sim} and R_E^{exp} for both EOS may be observed at the lowest E_{inc} only when the experimental errors are

accounted for. In addition, for the Zamick EOS, Fig. 1(b), the simulation strongly overshoots the data at the highest E_{inc} 's.

A full *ab initio* microscopic study of σ_{NN}^m based upon the Dirac-Brueckner approach to nuclear matter was performed by Li and Machleidt [16]. Besides dependence on energy, isospin, and density of $\sigma_{\text{NN}}^{\text{Cugnon}}$ for this $\sigma_{\text{NN}}^{\text{Li-Machleidt}}$, we have added an explicit dependence on angle. In contrast to the scattering of neutrons, which is taken as isotropic, those between neutron and proton σ_{np} and between protons σ_{pp} are anisotropic in accordance with the fit of Ref. [26], which is given in detail in the Appendix. Similarly to above, the corresponding values of R_E^{sim} are displayed by the blue curves and bluish zone in Fig. 1. Again, the compatibility of R_E^{sim} with R_E^{exp} is unsatisfactory. Nevertheless, for the D1-G1 EOS and $E_{\text{inc}} \lesssim E_F$, Fig. 1(a), the slope of the isotropy ratio excitation function is correct but the simulation somewhat undershoots the experimental points: R_E^{sim} may be taken as compatible with the lower edges of experimental errors on R_E^{exp} . For the Zamick EOS, Fig. 1(b), the compatibility with R_E^{exp} exists at low E_{inc} and around $E_{\text{inc}} \sim 60A$ MeV, but the general features of the data are poorly reproduced. Manifestly, none of the above parametrizations of σ_{NN}^m and EOS can account for the observed behavior of the R_E stopping observable in the full energy range.

The parameters in the above σ_{NN}^m are of a fixed value. By an expansion around the saturation value ρ_0 , Klakow *et al.* have suggested a simple parametrization for the dependence of σ_{NN}^m on the evolving nuclear density [27],

$$\sigma_{\text{NN}}^m = \sigma_{\text{NN}}^{\text{free}} \left(1 + \alpha \frac{\rho}{\rho_0} \right), \quad (6)$$

where ρ is evaluated locally according to Eq. (3), and α is a free parameter assumed to reduce the cross section, thus it is strictly negative. As before, for $\sigma_{\text{NN}}^{\text{free}}$ the value taken is the empirical $\sigma_{\text{NN}}^{\text{Chen}}$. The authors have recommended for α the domain $[-0.3, -0.1]$ [27]. In our simulation α is varied between -0.1 and -0.6 . These R_E^{sim} are presented in Fig. 1 by the thinner dashed curves with variable dash size. They display a more or less regular dependence on both E_{inc} and α . For the nonlocal EOS and $-0.6 \leq \alpha \leq -0.5$ the R_E^{exp} values at $E_{\text{inc}} \lesssim E_F$ are well reproduced in both slope and absolute value; cf. Fig. 1(a). At energies higher than E_F , however, for each E_{inc} another and regularly increasing value of the parameter α is required such that, at the highest E_{inc} here considered, it should become positive, implying an in-medium enhancement rather than a reduction of $\sigma_{\text{NN}}^{\text{free}}$ at $E_{\text{inc}} \gtrsim 80A$ MeV. Let us mention that R_E^{sim} with $\sigma_{\text{NN}}^{\text{Cugnon}}$ corresponds to that of $\sigma_{\text{NN}}^{\text{Klakow}}$ with $\alpha = -0.1$ in the full range of E_{inc} considered and for both EOS. Simulation results with $\sigma_{\text{NN}}^{\text{Li-Machleidt}}$ and D1-G1 EOS are compatible to $\sigma_{\text{NN}}^{\text{Klakow}}$ with $\alpha = -0.6$ and $E_{\text{inc}} \gtrsim 50A$ MeV. For the Zamick EOS of Fig. 1(b) one does not find a range of E_{inc} of stable value of the parameter α that gives

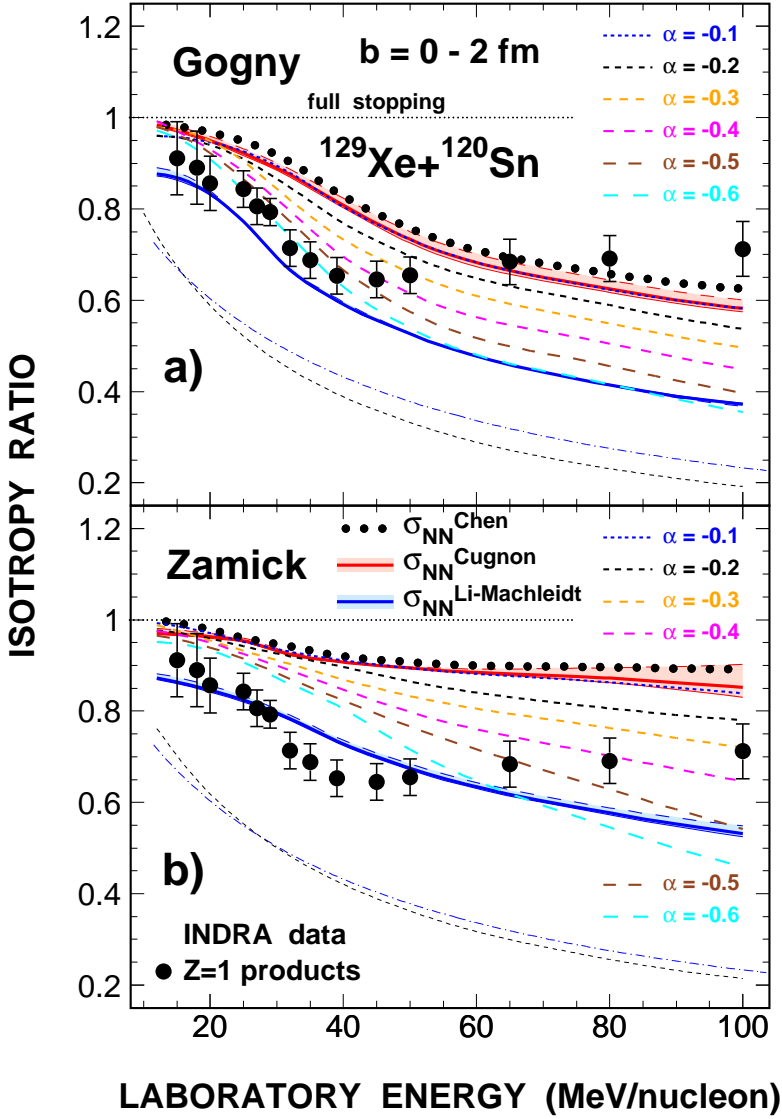


FIG. 1. (Color online.) Landau-Vlasov simulation results on the dependence of the transverse-to-longitudinal energy ratio R_E^{sim} of Eq. (5) as a function of incident energy for the central $^{129}\text{Xe} + ^{120}\text{Sn}$ reaction and several parametrizations of σ_{NN}^m . Panel (a) displays the results with the momentum dependent D1-G1 EOS and panel (b) those with the zero-range Zamick EOS. Heavy dotted curves represent the R_E^{sim} excitation function obtained with the $\sigma_{\text{NN}}^{\text{free}}$ due to Chen *et al.* [24]. The gray zones show the range of the R_E^{sim} -values limited by the impact parameter $b = 1$ fm (dashed bordering curves) and $b = 2$ fm (full bordering curves), while the heavy curve in each zone represents the b -weighted R_E^{sim} -values in the range $b = 0 - 2$ fm for σ_{NN}^m due to Cugnon *et al.* [25] (red curves and zones) and Li and Machleidt [16] (blue curves and zones). Thin dashed curves are obtained with the parametrization of σ_{NN}^m due to Klakow *et al.* [27] where the results for the different values of the parameter α of Eq. (6) are distinguished by the varied dash size and color. The filled circles and associated errors stand for the $Z = 1$ experimental R_E^{exp} values [7]. The thin dotted horizontal line denotes the full stopping value. The entrance channel values of R_E are shown by i) the thin dashed curve resulting from the two Fermi spheres ($E_F = 38$ MeV) displaced for the entrance channel relative momentum and ii) by the thin dash-dotted curves for the LV model values at the contact of colliding nuclei for each of the two EOS used.

R_E^{sim} 's compatible with either R_E^{exp} or those R_E^{sim} due to $\sigma_{\text{NN}}^{\text{Li-Machleidt}}$.

In conclusion, neither choice of σ_{NN}^m allows for a unique description of experimental observation. One faces the fact that every model study, ours and previous [8, 11–15], fails to reproduce with a single set of parameters the INDRA experimental results in the full energy range studied [4, 7]. In particular, all models but [15] predict steadily decreasing values of R_E^{sim} when E_{inc} increases, while experimental R_E^{exp} results display a break in the slope around the Fermi energy E_F .

B. Global modification of the free NN cross section

Being clearly unable to reproduce the experimental data with different parametrizations of the residual NN cross section, with or without momentum dependence of the force, let us concentrate on our second task that is, by following Ref. [7], to infer the multiplicative factor \mathcal{F}

between the in-medium NN cross section σ_{NN}^m and the free $\sigma_{\text{NN}}^{\text{free}}$ one:

$$\sigma_{\text{NN}}^m = \mathcal{F} \sigma_{\text{NN}}^{\text{free}}. \quad (7)$$

As previously done and as in [7], we take $\sigma_{\text{NN}}^{\text{free}} = \sigma_{\text{NN}}^{\text{Chen}}$ [24]. Of course, this simple cross-section normalization factor \mathcal{F} cannot completely describe the rather complex modification of the free NN interaction occurring in the nuclear medium. In particular, such a σ_{NN}^m is frozen during a reaction course and depends only indirectly on E_{inc} . Nevertheless, the prescription of Eq. (7) allows one to get an insight into the global in-medium effects on nuclear medium stopping properties and enables a comparison of the factor \mathcal{F}_{sim} obtained in our simulation with \mathcal{F}_{exp} of Ref. [7].

Figure 2 displays R_E^{sim} as a function of E_{inc} and the NN cross-section factor \mathcal{F} for the two effective interactions. In the D1-G1 EOS case, Fig. 2(a), the parameter \mathcal{F} takes values 0.2, 0.5, 0.8, 1.0, 1.2, and 1.5. For the Zamick EOS, Fig. 2(b), it is varied between 0.1 and 0.8

in steps of 0.1.¹ As in Fig. 1, R_E^{sim} are for central HIC with $b \leq 2.0$ fm, where $b=1$ fm (2 fm) results are represented by the thin dashed (full) curves that border the (colored) zone of each of the \mathcal{F} values. As before, the heavy curve in each zone shows the b -weighted R_E^{sim} that corresponds to 2% of σ_R . R_E^{sim} displays a regular dependence on E_{inc} and \mathcal{F} . In accordance with expectation and corroborating the results of Fig. 1, higher σ_{NN}^m (larger \mathcal{F}) implies higher stopping power of HICs. Unlike experimental R_E^{exp} and like our results of Fig. 1, as well as of a number of previous theoretical works [8, 11–15], the LV-simulation R_E^{sim} steadily decreases with E_{inc} for all \mathcal{F} without a minimum around E_F . At the lowest E_{inc} 's the mean field completely dominates the course of the collision, and for each \mathcal{F} value and both EOS R_E^{sim} is compatible with R_E^{exp} . For $E_{\text{inc}} \leq 45A$ MeV, R_E^{exp} is well reproduced by the $\mathcal{F}=0.5$ curve [Fig. 2(a)] and by the $\mathcal{F}=0.1$ one [Fig. 2(b)], respectively. Again, a single value of \mathcal{F} cannot reproduce experimental results. However, similarly to the case of the parameter α of Eq. (6), by allowing \mathcal{F} to change with E_{inc} one may find a set of \mathcal{F} values to achieve an agreement between R_E^{sim} and R_E^{exp} . The behavior of both the parameter α and the factor \mathcal{F} with E_{inc} corroborates the experimental finding [7] that the effective in-medium cross section σ_{NN}^m drastically changes with E_{inc} and that around E_F there is a break in this dependence.

We take the b -weighted R_E^{sim} as the starting point to infer information about the correction factor \mathcal{F} by which one would have to multiply $\sigma_{\text{NN}}^{\text{Chen}}$ to comply with R_E^{exp} . The procedure is evidenced in the inset of Fig. 3 in which the D1-G1 EOS at 50A MeV is shown as an example. The horizontal red line and reddish background zone display the R_E^{exp} value and its uncertainty, respectively, at 50A MeV. Blue circles joined by a broken line are the LV simulation R_E^{sim} as a function of \mathcal{F} at the same energy. The crossing of this broken line with the red line and the edges of the reddish zone give the most appropriate value for the factor \mathcal{F} of Eq. (7) and its uncertainty, respectively.

In the main panel of Fig. 3 we show, by the open circles and squares joined by dashed curves, the thus obtained \mathcal{F} values plotted against E_{inc} for the D1-G1 and Zamick EOS, respectively. Within experimental errors, the R_E^{sim} values for $E_{\text{inc}} \leq 20A$ MeV are roughly compatible with any \mathcal{F}^{exp} value and are not reported. The LV model with the highly recommended nuclear interaction D1-G1 for the range of energies of the present study and with the empirical NN cross section $\sigma_{\text{NN}}^{\text{Chen}}$ predicts, for all energies studied, about twice higher \mathcal{F} values compared to those suggested by Fig. 10 of Ref. [7]; these are presented in Fig. 3 as black filled circles, with the gray area showing their uncertainties. In contrast to this, when

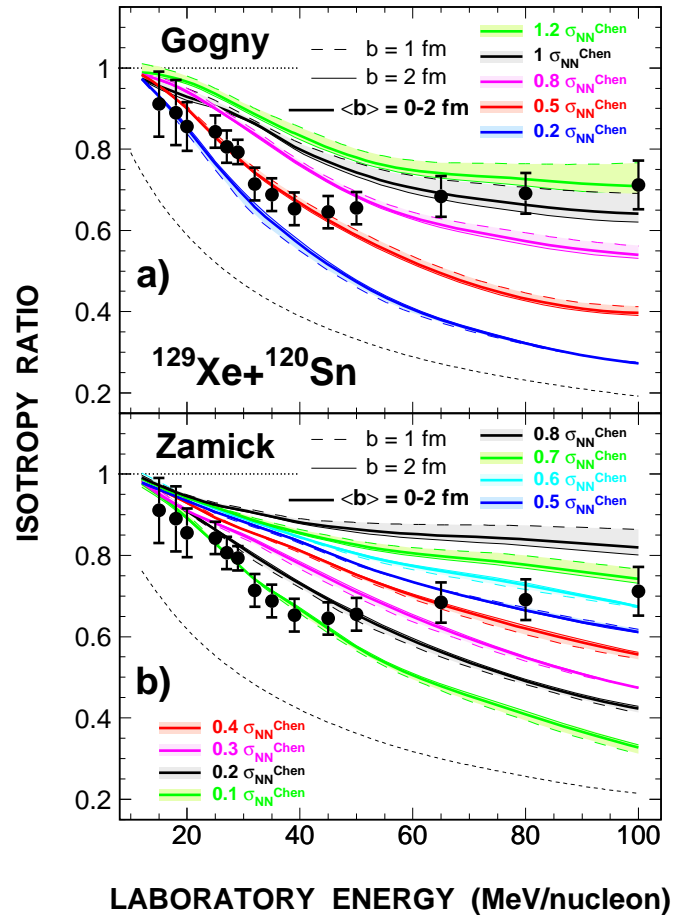


FIG. 2. (Color online.) R_E^{sim} as a function of incident energy for the central Xe + Sn reaction and several values of the $\sigma_{\text{NN}}^{\text{free}}$ scaling factor \mathcal{F} of Eq. (7). Upper (lower) panel shows results obtained with the D1-G1 (Zamick) EOS. The colored zones and curves have the same meaning as in Fig. 1, but here for the scaled σ_{NN} of Chen *et al.* [24]. For more details see the caption of Fig. 1 and the text.

experimental and simulation uncertainties are accounted for, the zero-range (*local*) Skyrme interaction in the Zamick implementation \mathcal{F}_{sim} is compatible with \mathcal{F}_{exp} above $E_{\text{inc}} \approx 35A$ MeV. Let us underline that \mathcal{F}_{sim} for both EOS display a minimum around E_F . The minimum is relatively more pronounced than the one suggested by \mathcal{F}_{exp} and it is somewhat shifted in energy. The Zamick EOS gives a \mathcal{F}_{sim} that reduces the free σ_{NN} at all E_{inc} while the D1-G1 EOS gives $\mathcal{F}_{\text{sim}} > 1$ at $E_{\text{inc}} \gtrsim 80A$ MeV.

C. Centrality versus multiplicity

The most evident difference between a simulation and an experimental data analysis is in the reliability of the assessments of reaction impact parameter b . Experimental selection of the most central collisions is made by assuming that there is a biunivocal correspondence between the reaction violence, i.e., the multiplicity of particles in

¹ Simulation was also performed for the pure mean field, i.e., the Vlasov equation with zeroed right-hand-side of Eq. (1), which is equivalent to taking the parameter $\mathcal{F}=0$.

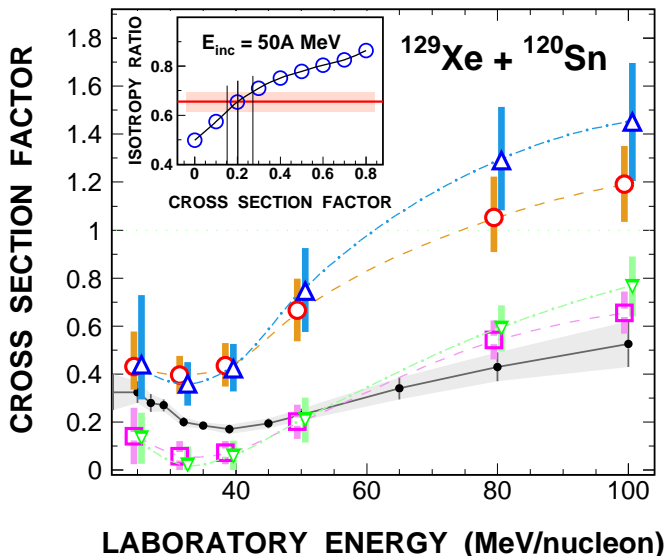


FIG. 3. (Color online.) Cross section correction factor \mathcal{F} of Eq. (7) as a function of E_{inc} . Open circles and squares interpolated by the dashed curve display \mathcal{F}_{sim} values obtained for R_E^{sim} evaluated in the $b=0-2$ fm range using the D1-G1 EOS and Zamick EOS, respectively. Open triangles, upright and reversed, interpolated by the dash-dotted curve denote the Gaussian weighted R_E^{sim} evaluated in the interval $b=0-5$ fm for the D1-G1 EOS and Zamick EOS, respectively. The symbols (but not the curves) are slightly shifted in E_{inc} to avoid overlapping error bars. Full dots, full curve, and gray zone represent \mathcal{F}_{exp} values and their uncertainty deduced from the experimental R_E^{exp} [7]. All curves are merely intended to guide the eye. The inset explains the procedure used to extract the values of \mathcal{F}_{sim} . For more details see text.

a reaction event, and the reaction centrality. In a simulation the centrality is an input variable, thus it is under full control. In comparing simulation results and the earlier INDRA study of R_E and R_p [4] it has been underlined that selecting events via multiplicity strongly mixes events of different impact parameters over a rather broad span in b [12, 28]. Thus, let us examine the b vs multiplicity relationship and its influence on the isotropy ratio. For that purpose we use the semidynamical general-purpose event-generating code HIPSE (Heavy-Ion Phase-Space Exploration) intended to describe HICs at intermediate energies [29]. At each energy 100 000 events are generated in the range $b=0-7$ fm. Let us note that, according to the expression of σ_R in Ref. [30], the above range in b is equivalent to $0.27\sigma_R-0.30\sigma_R$, depending on E_{inc} . At $E_{\text{inc}}=50A$ MeV the simulation was performed in the full impact parameter range of the $^{129}\text{Xe}+^{120}\text{Sn}$ reaction, i.e., $b=0-13$ fm, in order to verify that in the non-covered range ($b=7-13$ fm) the high multiplicity events, in which we are interested, are not present. By passing the generated events through a sophisticated INDRA-device geometry and detection-acceptance filter [31] we found that it has no appreciable effect on the $Z=1$ R_E values. Mostly, the change in R_E due to this

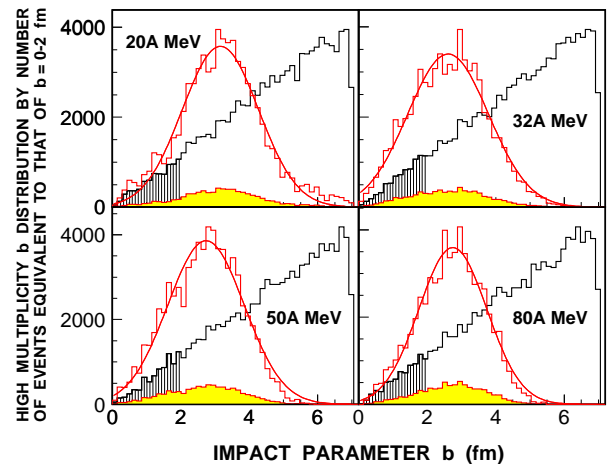


FIG. 4. (Color online.) Simulation of the $^{129}\text{Xe}+^{120}\text{Sn}$ reaction with the HIPSE code [29]. Shown are the b distributions of the full data set (black line) and of the high multiplicity subset (filled and hollow red-line histograms), which is by number of events equivalent to the one of $b=0-2$ fm (hatched part of the black histograms) for four E_{inc} . The curves are the best fits by a Gaussian function. For more details see text.

filter is below 0.5%.

Selecting the range $b=0-2$ fm, in a geometrical sharp-cut approximation, corresponds to 1.82% to 1.92% of σ_R in the studied E_{inc} range, i.e., between 104 and 116 mb. These values fall in the middle of the cross section values of the selected subset of the most violent INDRA data events analyzed in Ref. [7]. Ideally, the reactions with $b \leq 2$ fm should correspond to 8163 out of the total 100 000 generated events. In reality, there were on the average 8109 such events with a fluctuation up to 3% from energy to energy. We denote this precise number of events N_{0-2} to search for, in the full ensemble of 100 000 events, the subset of events with the highest multiplicity that is by number of events closest to N_{0-2} . By M_{0-2} we label both the lowest multiplicity of the thus selected subset as well as the subset of events itself at each E_{inc} .

Let us check the behavior of the most violent M_{0-2} HIPSE events. As a kind of "background", in Fig. 4 we show by the thin black line the b -distribution histogram of the full 100 000 event data set for each second studied E_{inc} . The b distribution of the M_{0-2} events is shown by the red-line yellow-filled histogram. These high-multiplicity events are generated in a large domain of b values which extends up to 5 fm. To make the M_{0-2} b distribution better visible, it is enlarged to the full frame size by the hollow red-line histogram. A Gaussian fit to it clearly demonstrates that the normal-law of data statistics correctly reproduces the distribution of M_{0-2} subset over b 's. These events are in minor part (3% to 29%) belonging to the $b \leq 2$ fm subset of the full data set (hatched part of black histogram). From the Gaussian fit one infers that the maximum of these high-multiplicity events is about $b \approx 3$ fm and that it slightly decreases with the increasing E_{inc} .

Finally, let us apply the HIPSE M_{0-2} b distribution to the LV simulation results. Taking the Gaussian fit values of Fig. 4 as the weights for the integer values of b , the b -averaged R_E^{sim} are obtained for each studied value of the factor \mathcal{F} of Eq. (7). By this method, for the $\mathcal{F}=1$ case these R_E^{sim} are, in millibarn units, also equivalent to $0.02\sigma_R$. \mathcal{F}^{sim} extracted from thus averaged R_E^{sim} is in Fig. 3 shown by dot-dashed curves and open triangles, upright and reversed, for the D1-G1 EOS and Zamick EOS, respectively. For the nonlocal D1-G1 EOS the two b -averaging intervals give strictly the same R_E^{sim} for $E_{\text{inc}} \leq 50A$ MeV. At $E_{\text{inc}} = 80A$ and $100A$ MeV the respective R_E^{sim} values differ by about 20% but are mutually compatible when errors are accounted for. For the zero-range Zamick EOS in the full E_{inc} interval, two b -averaging intervals give compatible predictions for the \mathcal{F}_{sim} values although for $E_{\text{inc}} \gtrsim E_F$ the more stringent centrality results are in somewhat better agreement with the \mathcal{F}_{exp} values.

IV. SUMMARY AND CONCLUSIONS

The semiclassical Landau-Vlasov (LV) transport model was used to study the energy-based isotropy ratio R_E of Eq. (5) for the $^{129}\text{Xe} + ^{120}\text{Sn}$ reaction in the wide incident energy range $12A \leq E_{\text{inc}} \leq 100A$ MeV. The focus of the present work is twofold:

- (1) the search for the set of model ingredients which most favorably describes the experimental values R_E^{exp} for the $Z=1$ species of Ref. [7] and
- (2) the comparison of the simulation multiplicative factor \mathcal{F} representing the global in-medium change of the free NN cross section $\sigma_{\text{NN}}^{\text{Chen}}$ of Ref. [24] with the one deduced from the experimental R_E^{exp} [7].

In approaching the above point 1 we investigated (i) the role of the dependence of the nuclear mean field on momentum, i.e., of the nonlocality of the interaction, and (ii) the impact of the residual NN interaction through varied parametrizations of σ_{NN} . The success in reproducing the experimental isotropy ratios R_E^{exp} of Ref. [7] is mixed: Below the Fermi energy E_F , the LV model with the strongly in-medium reduced NN cross section σ_{NN}^m of Refs. [16, 27] and with the momentum-dependent D1-G1 EOS leads to a correct description of R_E^{exp} ; cf. Fig. 1(a). A similar result may be obtained with both the D1-G1 EOS and the zero-range Zamick EOS when the free NN cross section is strongly scaled down by a constant multiplicative factor \mathcal{F} of Eq. (7): for the D1-G1 EOS $\mathcal{F} \sim 0.5$, Fig. 2(a), and for the Zamick EOS $\mathcal{F} \sim 0.1$, Fig. 2(b). Above E_F there is no unique set of model parameters which would lead to a favorable description of the experimental R_E^{exp} . Earlier studies of the observable R_E [8, 11–15] have also failed to reproduce the experimental results of Ref. [4]. We emphasize, however, that a smooth variation of the parameter that controls the in-medium value of σ_{NN} would lead to a complete description of the experimental R_E^{exp} for both EOS. Should one draw a con-

clusion that none of the existing studies on the in-medium modifications of σ_{NN} around the Fermi energy appropriately accounts for the physical reality? The local or the nonlocal character of the interaction does not elucidate this question.

Regarding the above point 2, we may summarize the outcome of our study as follows: the LV simulation with the local Zamick EOS predicts the NN cross-section correction factor \mathcal{F}_{sim} which clearly supports the experimentally deduced \mathcal{F}_{exp} [7]. The model predicts

- (1) an appreciable reduction of NN cross section all along the energy range of interest, as well as

- (2) the appearance of a break in the slope of the multiplicative factor \mathcal{F} after a minimum located near E_F .

However, the agreement or disagreement between the absolute values of \mathcal{F}_{sim} and \mathcal{F}_{exp} should be considered with some caution due to two possible causes. On one hand, the value of factor \mathcal{F} may be altered by reaction centrality. Accordingly, an investigation of R_E with a quasidynamical event generator HIPSE [29] was carried out. It reveals that the event selection based on multiplicity and the geometrical sharp-cut approximation is not a correct centrality selector. Indeed, corroborating earlier findings [12, 28], we show that this selection approach strongly mixes events of different impact parameters over a rather broad span of b values; cf. Fig. 4. When a properly weighted contribution of b 's involved in the high-multiplicity events is accounted for, the isotropy ratios calculated for the thus relaxed centrality requirement and those strictly central do not differ much. The thus extracted \mathcal{F}_{sim} does not change much as well. On the other hand, the derived \mathcal{F}_{exp} values are based on a number of strong assumptions that allowed the link between the stopping ratio R_E and the in-medium NN cross section [7]. Hence, besides further experimental and theoretical considerations of the stopping observable R_E intended to disentangle the remaining ambiguities a study of other related observables may shed some fresh light on the subject. In addition, the experimentally observed strong and rapid change of the effective in-medium residual NN cross section beyond the Fermi energy urges for an *ab initio* theoretical analysis of this problem, the solution of which might lie in the way the exclusion principle is accounted for [8] and/or by incorporating the recent observation of short-range correlations in nuclei [32, 33]. Their consequences for transport descriptions of heavy-ion reactions are of high interest and need to be investigated.

ACKNOWLEDGMENTS

Z.B. gratefully acknowledges the financial support and the warm hospitality of the Faculté des Sciences of University of Nantes and the Laboratory SUBATECH, UMR 6457. This work has been supported in part by Croatian Science Foundation under Project No. 7194 and in part by the Scientific Center of Excellence for Advanced Materials and Sensors.

TABLE I. Coefficients of neutron-proton scattering angular distribution function f_{np} of Eq. (A.2) as parametrized by Eqs. (A.3).

E (MeV)	e_i (MeV)	Ref.	$a_{i,1}$	$a_{i,2}$	$a_{i,3}$	$b_{i,1}$	$b_{i,2}$	$b_{i,3}$	c_i
$E < 26$	0		0	0	1	0	0	0	1
$26 \leq E < 35$	26	[34]	0	0	1	0.966	-0.426	1.372	9
$35 \leq E < 45$	35	[35]	0.97	-0.426	2.372	0.32	0.35	-0.40	10
$45 \leq E < 53$	45	[35]	1.29	-0.073	1.97	0.32	-0.127	-0.18	8
$53 \leq E < 63$	53	[35]	1.61	-0.2	1.79	-0.04	0.51	0.16	10
$63 \leq E < 73$	63	[35-37]	1.57	0.31	1.95	0.33	-0.59	-0.30	10
$73 \leq E < 90$	73	[35]	1.9	-0.28	1.65	0.9	0.205	-0.16	17
$90 \leq E < 130$	90	[36, 38]	2.8	-0.075	1.49	1.2	-0.465	-0.094	40
$130 \leq E < 319$	129	[39]	4.0	-0.54	1.396	-1.3	0.665	-0.81	189
$E \geq 319$	319	[40]	2.69	0.125	0.588	0	0	0	1

Appendix

The angular dependence of the nucleon-nucleon (NN) cross section σ_{NN} is expressed as

$$\sigma(\theta)_{\text{c.m.}}(\text{mb/sr}) = f(E, \theta) \times \frac{\sigma_{\text{tot}}(\text{mb})}{4\pi}, \quad (\text{A.1})$$

where $\sigma_{\text{tot}} = \sigma_{\text{NN}}^{\text{Li-Machleidt}}$ is the total elastic cross section due to Li and Machleidt [16]. The dimensionless weighting factor $f(E, \theta)$ is equal to unity for the scattering between neutrons ($f_{\text{nn}} \equiv 1$) and is increasingly anisotropic as energy increases for neutron-proton scattering (the f_{np} case), and especially becomes strongly forward-backward peaked for the scattering between protons (f_{pp}). The parametrization of the angular dependence of σ_{np} is defined as [26]

$$f(E, \theta)_{\text{np}} = \frac{A_1 \cos^4 \theta - A_2 \cos^3 \theta + A_3}{A_1/5 + A_3}, \quad (\text{A.2})$$

where, for the purpose of the fitting, the coefficients A_k at each energy are expressed by the following functional dependence:

TABLE II. Coefficients of proton-proton scattering angular distribution function f_{pp} of Eq. (A.4) as parametrized by Eqs. (A.5).

E (MeV)	ϵ_i (MeV)	Ref.	$\alpha_{i,1}$	$\alpha_{i,2}$	$\alpha_{i,3}$
$E < 5$	0		5176.1	-8.91	100.0
$5 \leq E < 9.9$	5	[41]	5176.1	-8.91	100.0
$9.9 \leq E < 19.7$	9.9	[42]	1795.6	-9.29	52.62
$19.7 \leq E < 39.4$	19.7	[43]	1071.0	-12.0	24.95
$39.4 \leq E < 68$	39.4	[44]	1382.2	-19.26	11.16
$68 \leq E < 144$	68	[45]	1880.5	-26.77	6.16
$E \geq 144$	144	[46]	4008.8	-45.92	3.99

$$A_k(E) = a_{i,k} + \frac{b_{i,k}(E - e_i)}{c_i}, \quad k = 1, 2, 3. \quad (\text{A.3})$$

Parameters $a_{i,k}$, $b_{i,k}$, and c_i are fixed by fitting the experimental σ_{np} data at nine beam energies e_i between 26 and 319 MeV, index i running over energies. E and e_i are expressed in MeV units. Between these e_i values the parameters are assumed to change linearly with E . The values of these parameters are given in Table I and $f(E, \theta)_{\text{np}}$ is shown in Fig. 5(a).

Adopting a very crude estimate, the polar angle dependence of σ_{pp} is defined as [26]

$$f(E, \theta)_{\text{pp}} = \begin{cases} B_1 \exp(B_2 \theta), & \theta < \theta_0, \\ B_3, & \theta_0 < \theta < \pi - \theta_0, \\ B_1 \exp(B_2(\pi - \theta)), & \theta > \pi - \theta_0, \end{cases} \quad (\text{A.4})$$

where coefficients B_k are expressed by the following functional dependence:

$$B_k(E) = \alpha_{i,k} + \frac{(\alpha_{i+1,k} - \alpha_{i,k})(E - \epsilon_i)}{\epsilon_{i+1} - \epsilon_i}, \quad k = 1, 2, 3. \quad (\text{A.5})$$

Due to indistinguishability of particles, coefficients B_1 and B_3 are divided by 2. At each energy E the limiting angle reads $\theta_0 = \ln(B_3/B_1)/B_2$. The overall angular distribution normalization is given by the value of $\sigma_{\text{pp}}^{\text{Li-Machleidt}}$, and Eq. (A.4) is used to define, on Monte Carlo grounds, the angle into which a couple of charged Gaussians is scattered in a $p-p$ collision. The parameters $\alpha_{i,k}$ are fixed by fitting experimental differential cross sections σ_{pp} at six energies ϵ_i ranging from 5 to 144 MeV denoted by the index i . As above, E and ϵ_i are expressed in MeV units. Between these energies, parameters are assumed to change linearly with E . The values of these parameters are given in Table II and $f(E, \theta)_{\text{pp}}$ is shown in Fig. 5(b).

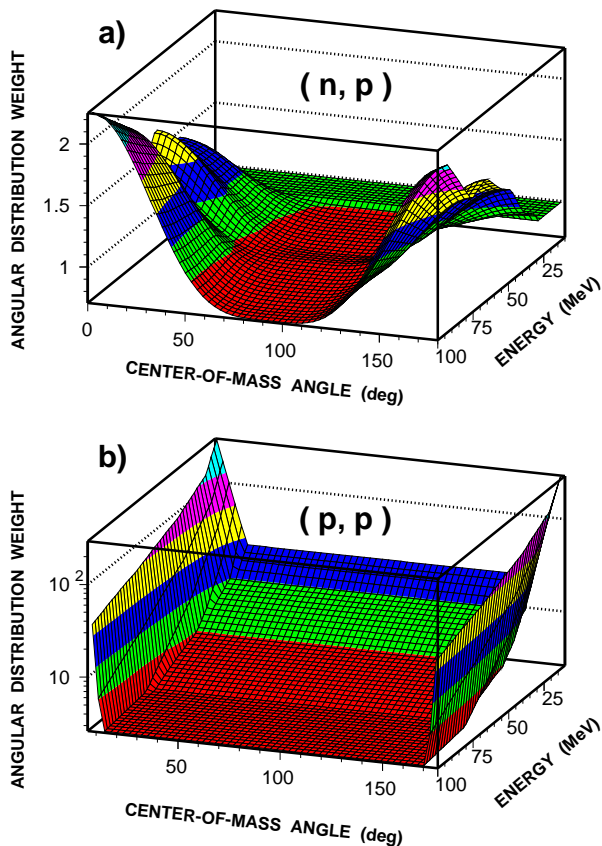


FIG. 5. (Color online.) Dimensionless weighting factor $f(E, \theta)$ which modulates total elastic cross section as a function of polar angle $\theta_{c.m.}$ and nucleon incident energy E for the scattering of neutron and proton (upper panel) and between protons (lower panel), where the applicate axis is logarithmic scale.

-
- [1] H. Ströbele *et al.*, Phys. Rev. C **27**, 1349 (1983).
[2] W. Bauer, Phys. Rev. Lett. **61**, 2534 (1988).
[3] B. Hong *et al.* (FOPI Collaboration), Phys. Rev. C **66**, 034901 (2002); W. Reisdorf *et al.* (FOPI Collaboration), Phys. Rev. Lett. **92**, 232301 (2004).
[4] G. Lehaut *et al.* (INDRA Collaboration), Phys. Rev. Lett. **104**, 232701 (2010).
[5] P. Eudes *et al.*, Europhys. Lett. **104**, 22001 (2013).
[6] P. Eudes *et al.*, Phys. Rev. C **90**, 034609 (2014).
[7] O. Lopez *et al.* (INDRA Collaboration), Phys. Rev. C **90**, 064602 (2014).
[8] In the work by J. Su and F.-S. Zhang [Phys. Rev. C **87**, 017602 (2013)] the same observable is dubbed the memory loss ratio.
[9] P. Eudes *et al.*, Phys. Rev. C **56**, 2003 (1997);
[10] F. Haddad *et al.*, Phys. Rev. C **60**, 031603 (1999);
[11] Jian-Ye Liu *et al.*, Phys. Rev. Lett. **86**, 975 (2001).
[12] G. Q. Zhang *et al.*, Phys. Rev. C **84**, 034612 (2011).
[13] V. Kaur, S. Kumar, and R. K. Puri, Nucl. Phys. A **861**, 37 (2011).
[14] K. S. Vinayak and S. Kumar, J. Phys. G **39**, 095105 (2012).
[15] M. H. Zhao *et al.*, Phys. Rev. C **89**, 037001 (2014).
[16] G.Q. Li and R. Machleidt, Phys. Rev. C **49**, 566 (1994); **48**, 1702 (1993).
[17] C. Grégoire *et al.*, Nucl. Phys. A **465**, 317 (1987).
[18] F. Sébille *et al.*, Nucl. Phys. A **501**, 137 (1989).
[19] J. Dechargé and D. Gogny, Phys. Rev. C **21**, 1568 (1980).
[20] L. Zamick, Phys. Lett. B **45**, 313 (1973).
[21] F. Haddad *et al.*, Phys. Rev. C **52**, 2013 (1995).
[22] P. Schuck *et al.*, Prog. Part. Nucl. Phys. **22**, 181 (1989); V. de la Mota *et al.*, Phys. Rev. C **46**, 677 (1992); F. Haddad *et al.*, *ibid.* **53**, 1437 (1996); Z. Basrak *et al.*, Nucl. Phys. A **624**, 472 (1997); I. Novosel *et al.*, Phys. Lett. B **625**, 26 (2005).
[23] L. W. Nordheim, Proc. Roy. Soc. **A119**, 689 (1928); E. A. Uehling and G. E. Uhlenbeck, Phys. Rev. **43**, 552 (1933).
[24] K. Chen *et al.*, Phys. Rev. **166**, 949 (1968).
[25] J. Cugnon, A. Lejeune, and P. Grangé, Phys. Rev. C **35**, 861 (1987).
[26] F. Sébille *et al.*, Nucl. Phys. A **791**, 313 (2007); F. Sébille, private communication.

- [27] D. Klakow, G. Welke and W. Bauer, Phys. Rev. C **48**, 1982 (1993); D. J. Magestro, W. Bauer, and G. D. Westfall, *ibid.* **62**, 041603(R) (2000).
- [28] E. Bonnet *et al.*, Phys. Rev. C **89**, 034608 (2014).
- [29] D. Lacroix, A. Van Lauwe, and D. Durand, Phys. Rev. C **69**, 054604 (2004).
- [30] R.K. Tripathi, F.A. Cucinotta, and J.W. Wilson, Nucl. Instr. Meth. Phys. Res. B **117**, 347 (1996).
- [31] P. Napolitani (napolita@ipno.in2p3.fr), code *Panforte* for simulating geometrical and detailed detection features of several multidetectors.
- [32] R. Subedi *et al.*, Science **320**, 1476 (2008).
- [33] O. Hen *et al.*, Science **346**, 614 (2014).
- [34] T.C. Montgomery *et al.*, Phys. Rev. C **16**, 499 (1977).
- [35] S. Benck *et al.*, Nucl. Phys. A **615**, 220 (1997).
- [36] J.P. Scanlon *et al.*, Nucl. Phys. **41**, 401 (1963).
- [37] N.S.P. King *et al.*, Phys. Rev. C **21**, 1185 (1980).
- [38] C.Y. Chih and W.M. Powell, Phys. Rev. **106**, 539 (1959).
- [39] D.F. Measday, Phys. Rev. **142**, 584 (1966).
- [40] R.K. Keeler *et al.*, Nucl. Phys. A **377**, 529 (1982).
- [41] R.E. Meagher, Phys. Rev. **78**, 667 (1950).
- [42] N. Jarmie *et al.*, Phys. Rev. Lett. **25**, 34 (1970).
- [43] N. Jarmie and J.H. Jett, Phys. Rev. C **13**, 2554 (1976).
- [44] L.H. Johnston and D.A. Swenson, Phys. Rev. **111**, 212 (1958).
- [45] D.E. Young and L.H. Johnston, Phys. Rev. **119** 313 (1960).
- [46] O.N. Jarvis and C. Whitehead, Phys. Lett. B **36**, 409 (1971).